NeuroImage: Clinical 23 (2019) 101879

Contents lists available at ScienceDirect

NeuroImage: Clinical

journal homepage: www.elsevier.com/locate/ynicl

Multiparameter MRI quantification of microstructural tissue alterations in multiple sclerosis

Emilie Lommers[a,b,*], Jessica Simon[c], Gilles Reuter[a,d], Gaël Delrue[b], Dominique Dive[b], Christian Degueldre[a], Evelyne Balteau[a], Christophe Phillips[a,e], Pierre Maquet[a,b]

[a] GIGA – CRC in vivo Imaging, University of Liège, Liège, Belgium
[b] Clinical Neuroimmunology Unit, Neurology Department, CHU Liège, Belgium
[c] Psychology and Neurosciences of Cognition Research Unit, University of Liège, Belgium
[d] Neurosurgery Department, CHU Liège, Belgium
[e] GIGA – in silico Medicine, University of Liège, Liège, Belgium

ARTICLE INFO

Keywords:
Multiple sclerosis
Quantitative MRI
Histological MRI
Relaxometry

ABSTRACT

Objectives: Conventional MRI is not sensitive to many pathological processes underpinning multiple sclerosis (MS) ongoing in normal appearing brain tissue (NABT). Quantitative MRI (qMRI) and a multiparameter mapping (MPM) protocol are used to simultaneously quantify magnetization transfer (MT) saturation, transverse relaxation rate R2* (1/T2*) and longitudinal relaxation rate R1 (1/T1), and assess differences in NABT microstructure between MS patients and healthy controls (HC).

Methods: This prospective cross-sectional study involves 36 MS patients (21 females, 15 males; age range 22–63 years; 15 relapsing-remitting MS - RRMS; 21 primary or secondary progressive MS - PMS) and 36 age-matched HC (20 females, 16 males); age range 21–61 years). The qMRI maps are computed and segmented in lesions and 3 normal appearing cerebral tissue classes: normal appearing cortical grey matter (NACGM), normal appearing deep grey matter (NADGM), normal appearing white matter (NAWM). Individual median values are extracted for each tissue class and MR parameter. MANOVAs and stepwise regressions assess differences between patients and HC.

Results: MS patients are characterized by a decrease in MT, R2* and R1 within NACGM ($p < .0001$) and NAWM ($p < .0001$). In NADGM, MT decreases ($p < .0001$) but R2* and R1 remain normal. These observations tend to be more pronounced in PMS. Quantitative MRI parameters are independent predictors of clinical status: EDSS is significantly related to R1 in NACGM and R2* in NADGM; the latter also predicts motor score. Cognitive score is best predicted by MT parameter within lesions.

Conclusions: Multiparametric data of brain microstructure concord with the literature, predict clinical performance and suggest a diffuse reduction in myelin and/or iron content within NABT of MS patients.

1. Introduction

Multiple sclerosis (MS) is a chronic immune-mediated disease of the central nervous system (CNS). The course of the disease seems driven by two distinct clinical phenomena: the alternation of relapses and remissions on the one hand, and the steady and irreversible worsening of the clinical status, or progression, on the other hand (Reich et al. 2018). These processes are differently expressed in individual patients leading to the identification of relapsing–remitting MS (RRMS), secondary progressive MS (SPMS) and primary progressive MS (PPMS) (Miller and Leary 2007; Reich et al. 2018).

In clinical practice, Magnetic Resonance Imaging (MRI), albeit sensitive to focal lesions on T2-weighted sequences, does not usefully characterize normal appearing grey and white matters (NAGM and NAWM, respectively) and is insensitive to most pathological processes underpinning MS (Filippi et al. 2012; Zivadinov and Leist 2005). Consequently, correlations between total lesion load and clinical measures are generally modest (Barkhof 2002). Quantitative MRI potentially overcomes these limitations by a direct noninvasive quantification of microstructural changes in normal appearing brain tissues (NABT), particularly pronounced and diffuse in progressive MS (PMS) (Enzinger et al. 2015; Kutzelnigg et al. 2005).

This prospective cross-sectional study aims at revisiting differences in microstructure in three tissue classes of NABT (normal appearing

* Corresponding author at: Department of Neurology, CHU Liège, Avenue Hippocrate, 4000 Liège 1, Belgium.
E-mail address: elommers@chuliege.be (E. Lommers).

https://doi.org/10.1016/j.nicl.2019.101879
Received 29 January 2019; Received in revised form 23 April 2019; Accepted 25 May 2019
Available online 29 May 2019

Nomenclature

BPF	Brain Parenchymal Fraction
GMF	Grey Matter Fraction
HC	Healthy Controls
LF	Lesion Fraction
MPM	Multiparameter mapping
MRI	Magnetic Resonance Imaging
MS	Multiple Sclerosis
MT	Magnetization Transfer
MTR	Magnetization Transfer Ratio
NABT	Normal Appearing Brain Tissue
NACGM	Normal Appearing Cortical Grey Matter
NADGM	Normal Appearing Deeps Grey matter
NAWM	Normal Appearing White Matter
NAGT	Normal Appearing Grey Tissue
RRMS	Relapsing-Remitting Multiple Sclerosis
PMS	Progressive Multiple Sclerosis
R1	Longitudinal Relaxation Rate R1 (1/T1)
R2*	Transverse Relaxation Rate R2* (1/T2*)
TIV	Total Intracranial Volume

cortical and deep grey matters - NACGM and NADGM, respectively, and NAWM), between MS patients (both RRMS and PMS) and healthy controls (HC), using a multiparameter mapping (MPM) protocol which simultaneously quantitates MT saturation, R2* and R1 with high resolution and whole brain coverage (Callaghan et al. 2014; Draganski et al. 2011; Tabelow et al. 2019; Weiskopf et al. 2013). We also explore whether these parameters predict motor and cognitive functions in MS patients.

2. Materials and methods

2.1. Patients

Seventy-two participants took part in this study, which was approved by the local ethic committee (approval number B707201213806). Written informed consent was obtained from all participants. Thirty-six patients were recruited at the specialized MS outpatient clinic of the CHU Liège, Belgium, with a diagnosis of MS according to McDonald criteria 2010 (Polman et al. 2011). The inclusion criteria were (1) age between 18 and 65 years, (2) Expanded Disability Status Scale (EDSS) inferior or equal to 6.5; (3) absence of relapse within the previous 4 weeks; (4) Compatibility with MRI. Patients were classified as relapsing-remitting MS (15 RRMS) or progressive MS (primary and secondary progressive – 21 PMS). Twenty-one patients were receiving disease-modifying treatments (DMTs; 11 first lines, 8 second lines, 2 non-validated therapies). Thirty-six healthy control (HC) participants, matched for age and gender, free from neurological or psychiatric disease, followed the exact same experimental protocol. Demographic data appear in Table 1.

Patients with MS were scored by a qualified MS specialist (EL) on the EDSS, Time 25-Foot Walk (T25FW), 9-Hole Peg Test (9-HPT) of both hands, oral Symbol Digit Modalities test (SDMT) and five recalls of California Verbal Learning Test (CVLT). *Z*-scores for T25FW, 9-HPT, SDMT and CVLT were standardized to HC summary statistics and transformed to make improvement a positive number. Finally, a motor ($[Z_{T25FW} + Z_{9\text{-HPT dominant hand}} + Z_{9\text{-HPTnon dominant hand}}]/3$) and cognitive ($[Z_{SDMT} + Z_{CVLT}]/2$) composite scores were computed.

2.2. MR image acquisition

MRI data were acquired either on a 3 T head-only MRI-scanner (Magnetom Allegra, Siemens Medical Solutions, Erlangen, Germany) or on a 3 T whole-body MRI-scanner (Magnetom Prisma, Siemens Medical Solutions, Erlangen, Germany). The whole-brain MRI acquisitions included a MPM protocol, developed in the framework of an international collaborative effort (Draganski et al. 2011; Tabelow et al. 2019). This protocol consists of three co-localized 3D multi-echo fast low angle shot (FLASH) acquisitions at $1 \times 1 \times 1\,mm^3$ resolution and two additional calibration sequences to correct for inhomogeneities in the RF transmit field (Lutti et al., 2010, 2012). The FLASH data sets were acquired with predominantly proton density (PD), T1 and MT weighting, referred to in the following as PDw, T1w and MTw echoes. All three had high bandwidth to minimize off-resonance and chemical shift artifacts. Volumes were acquired in 176 sagittal slices using a 256×224 voxel matrix. GRAPPA parallel imaging was combined with partial Fourier acquisition to speed up acquisition time to approximately 20 min. Details of the MPM protocol used for this study are available in supplementary data. An additional FLAIR sequence was recorded with spatial resolution $1 \times 1 \times 1\,mm^3$ and TR/TE/TI = 5000 ms/516 ms/1800 ms.

2.3. MRI imaging processing

All data analyses and processing were performed in Matlab (The MathWorks Inc., Natick, MA, USA) using SPM12 (www.fil.ion.ucl.ac.uk/spm) and three additional dedicated SPM-extension toolboxes: *LST* version 1.2.3 (www.statisticalmodelling.de/lst.html) (Schmidt et al. 2012), *hMRI* (http://hmri.info) (Tabelow et al. 2019) and *USwithLesion* (https://github.com/CyclotronResearchCentre/USwLesion).

MT saturation, R2* and R1 quantitative maps were estimated using the *hMRI* toolbox, which also generates proton density map (PD*). We chose not to use the latter, due to a potential residual T2* weighting. Echoes for T1w, PDw and MTw were extrapolated to TE = 0 to increase

Table 1
Demographic data.

	All patients (n = 36)	RRMS (n = 15, 41.6%)	SPMS (n = 7, 18.4%)	PPMS (n = 14, 38.8%)	HC (n = 36)
Age, y, mean (SD)	45.69 (11.85)	36.53 (9.32)[a,b]	50.14 (6.46)	53.28 (9.78)	45.86 (12.45)
Sex, n (%)					
Males	15 (41.7)	6 (40)	0 (0)	9 (64.3)	16 (44.44)
Females	21 (58.3)	9 (60)	7 (100)	5 (35.7)	20 (55.55)
Disease duration, y, median (range)	13 (0.5–35)	6 (0.5–28)	21 (9–35)	12.5 (2–35)	N/A
Baseline EDSS, median (range)	4 (1–6.5)	2 (1–5.5)[a]	4 (3.5–6)	4.75 (3–6.5)	
Number of relapses, median (range)	1.5 (0–10)	4 (1–6)	10 (2–10)	0	

Abbreviations: RRMS = relapsing-remitting multiple sclerosis, SPMS = secondary progressive multiple sclerosis, PPMS = primary progressive multiple sclerosis, PMS = progressive multiple sclerosis (SPMS and PPMS), HC = healthy controls.

[a] Difference between RRMS and PMS statistically significant (alpha value of 0.05).

[b] Difference between RRMS and HC statistically significant (alpha value of 0.05).

the signal-to-noise ratio and get rid of the otherwise remaining R2* bias (Balteau et al. 2018; Weiskopf et al. 2014). The resulting MTw and T1w (TE = 0) images were used to calculate MT saturation and R1 quantitative maps. R1 maps were corrected for local RF transmit field inhomogeneities and imperfect RF spoiling using the approach described by Preibisch and Deichmann (Preibisch and Deichmann 2009) which was adapted to the FLASH acquisition parameters used here. The MT saturation map differs from the commonly used MT ratio (MTR, percent reduction in steady state signal) by explicitly accounting for spatially varying T1 relaxation time and flip angles. MT saturation shows a higher brain contrast to noise ratio than the MTR, leading to improved and more robust segmentation in healthy subjects (Helms et al. 2010). The R2* map was estimated from all three multi-echo series using the ESTATICS model (Weiskopf et al. 2014). Example maps are shown in Fig. 1. Note that these MR sequences at 3 Tesla are not sensitive to cortical lesions as described in (Filippi et al. 2013; Hulst and Geurts 2011) although a few lesions at the cortico-subcortical border (cortical lesions Type I) were detected. Quantification of cortical parameters is thus confounded by a minority of voxels potentially located within cortical lesions.

Quantitative maps of MS patients were segmented with the *USwithLesion* toolbox, in different cerebral tissue classes: normal appearing cortical grey matter (NACGM), normal appearing deep grey matter (NADGM), normal appearing white matter (NAWM) and lesions. The presence of focal demyelinated lesions required improvement of automated segmentation procedure available in SPM software that uses the tissue contrast in the image(s) and *a priori* tissue probability maps (TPM) (Ashburner and Friston 2005). We followed a multi-step procedure for each patient individually (Phillips et al., 2017). A preliminary lesion mask was generated from FLAIR and T1 weighted images by the lesion growth algorithm (Schmidt et al. 2012) as implemented in the *LST* toolbox. Optimal initial threshold kappa was determined by visual inspection. Manual corrections were performed when necessary. Based on this binary lesion mask, the *USwithLesion* toolbox generated a patient specific TPM by adding an extra lesion tissue class to MPM dedicated TPM (Lorio et al. 2016) and updating the white matter prior map accordingly (Moon et al. 2002). The individual number lesions impinging upon the cortical ribbon was so low that we did not update the grey matter TPM. Importantly small inaccuracies in this preliminary mask were smoothed out during the update of the TPM. A multi-channel unified segmentation approach (Ashburner and Friston 2005) using multiple contrast images (FLAIR, MT, R2*, R1) was then applied to MR images with these updated patient-specific TPM. The outputs were the segmented tissue classes (*a posteriori* tissue probability maps, including lesions) and spatial warping into standard template space (Fig. 2). For HC, multi-channel unified segmentation was applied with the same MPM specific TPM (Lorio et al. 2016).

For each participant, a set of three qMRI parameters (MT, R2*, R1) were extracted from all voxels of the 3 tissue classes (NACGM, NADGM, NAWM), based on a 90% probability to belong to the tissue class. Lesions were considered as an additional tissue class for patients. The brainstem and cerebellum were excluded because of unsatisfactory GM segmentation. Summary measurements were computed for each subject as median values for each tissue class and each qMRI parameter (Table 2). In addition, the following measures of brain volume were generated: Total intra-cranial volume (TIV) = volume (NAWM + GM + CSF + lesions), brain parenchymal fraction (BPF) = volume (NAWM + GM + lesions)/TIV, GM fraction (GMF) = volume (GM/TIV), lesion fraction (LF) = volume (lesion/TIV) (Table 2).

2.4. Statistical analyses

Statistical analyses were computed using SAS software, Version 9.4 (SAS Institute Inc., 2013).

For demographic data, group differences in brain volume, age and disease duration were assessed using one-way analyses of variance (ANOVA). Between-group differences in gender ratio were estimated by χ^2. RRMS and PMS differences for clinical data were investigated with Wilcoxon rank-sum test (EDSS) and ANOVA (motor and cognitive score).

Due to the influence of normal aging on brain microstructure (Callaghan et al. 2014; Draganski et al. 2011), quantitative parameters were all first corrected for age. Residuals of this preliminary analysis were used in subsequent statistical analyses.

Three two-way multivariate analyses of variance (MANOVA), one for each parameter (MT, R2* and R1), estimated the effects of group (HC, RRMS, PMS) and tissue class (NACGM, NADGM, NAWM), with scanner as independent variable of no interest. Tukey's post-hoc analyses were performed when necessary to explore significant principal effects. We consider an alpha level for statistical significance at 0.05.

The relationship of qMRI parameters to volumetric data was evaluated using Bravais-Pearson's correlation coefficient in the two MS groups. Inferences were performed at an alpha level for statistical significance at 0.01.

A stepwise regression including age (forced), scan (forced), gender, disease duration, lesion fraction and all qMRI features, looked across all

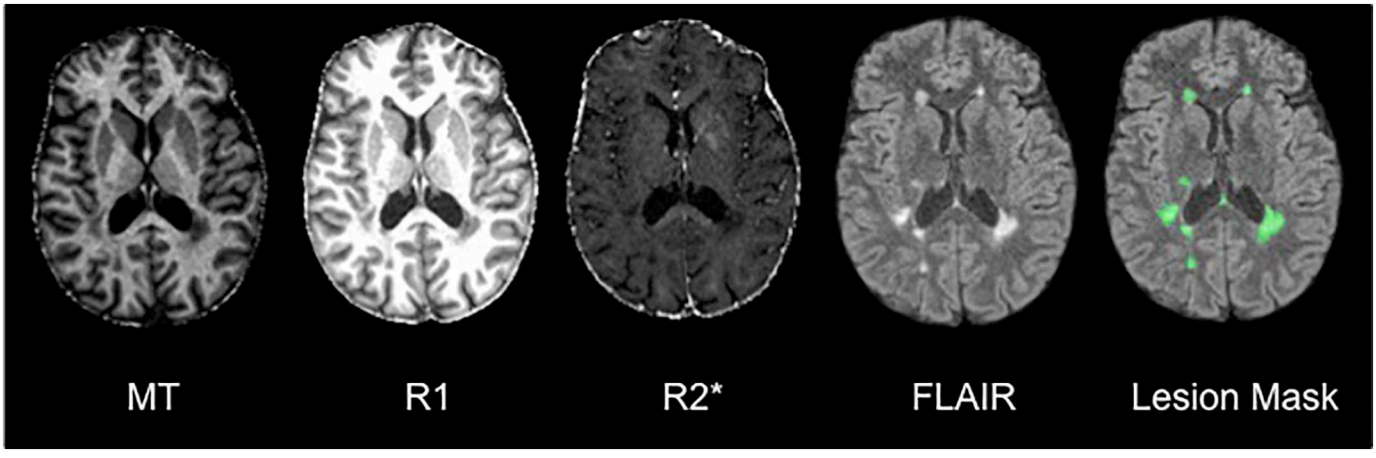

Fig. 1. Example of MPM quantitative maps for a specific MS patient.
From left to right: 3 MPM quantitative maps (MT, R1, R2*), standard FLAIR sequence image, and FLAIR image overlaid with the estimated lesion mask. MT = magnetization transfer saturation, R1 = longitudinal relaxation rate (1/T1), R2* = effective transverse relaxation rate (1/T2*). Lesion mask = posterior probability map of lesion tissue thresholded at 90%.

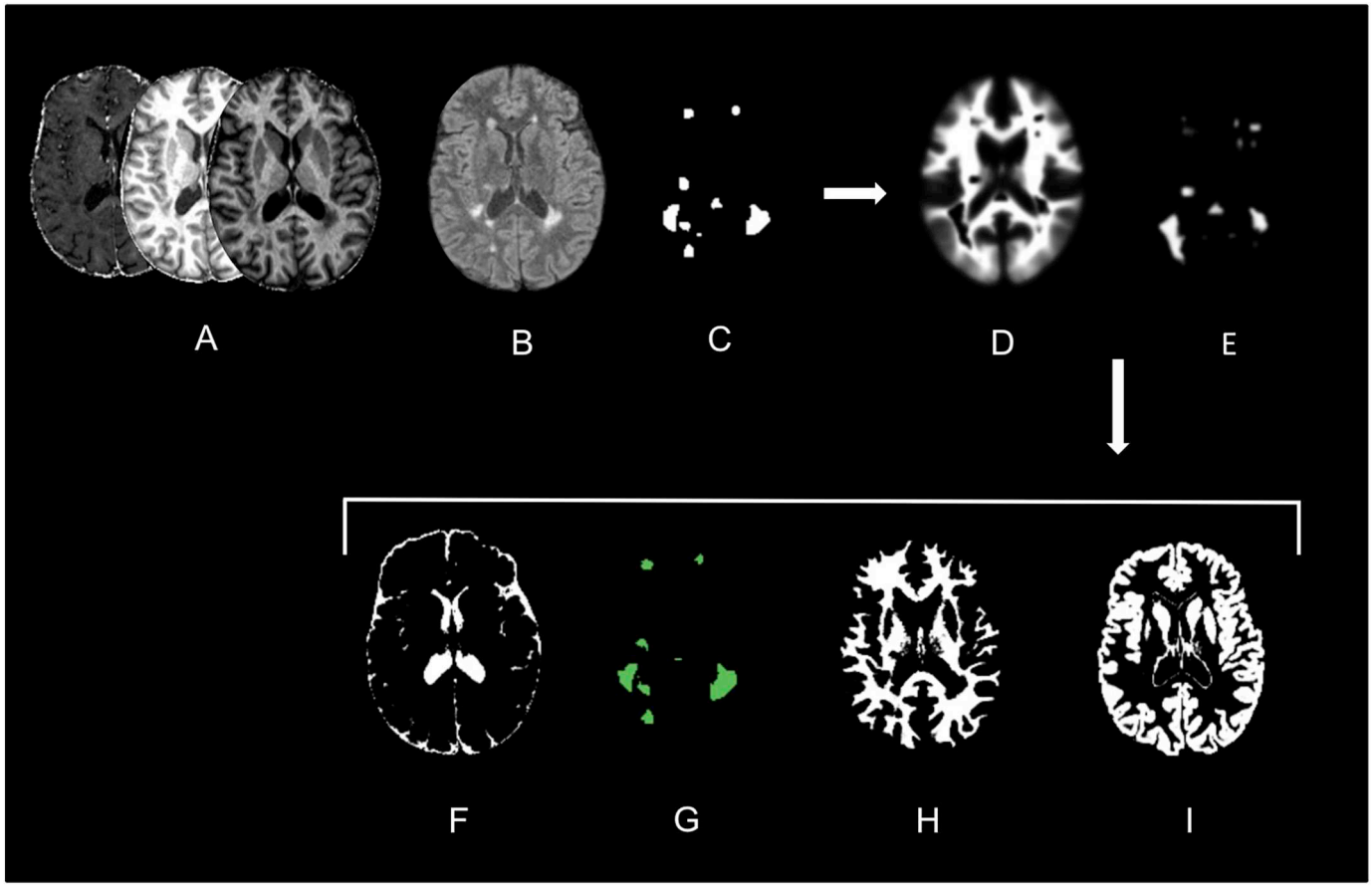

Fig. 2. Example of *USwithLesion* toolbox application on a specific MS patient.
(A) 3 MPM quantitative maps (MT, R1, R2*); (B) FLAIR-weighted MR images; (C) approximate binary lesion mask; (D, E) updated WM and lesion prior probability maps; (F-I) *a posteriori* probability maps for CSF, lesion, WM and GM tissue classes.

patients for the best predictors of clinical scores (motor score, cognitive score and EDSS).

2.5. Data availability

MR data supporting the results of this study are available from the corresponding author, on a collaborative basis.

3. Results

Patients and HC did not differ by age ($F(1,70) = 0.00$, $p = .95$). However, RRMS patients were younger than PMS patients and HC ($F(2,69) = 9.26$ $p < .001$). The three groups matched in terms of gender ($\chi^2 = 0.26$, $p = .88$). Disease duration was similar in the two patient groups ($F(1,34) = 3.72$ $p = .06$) (Table 1). PMS patients were clinically more impaired than RRMS patients with higher EDSS ($S = 174$ $p < .001$) and lower motor ($F(1,34) = 13.62$ $p = .01$) and cognitive ($F(1,34) = 5.76$ $p = .02$) composite scores. We observed a principal group effect on BPF ($F(2,69) = 4.76$, $p = .01$) and GMF ($F(2,69) = 20.81$, $p < .001$) with lower volumes in PMS patients than HC. No significant differences were observed for RRMS although these two volume fractions tend to be reduced compared to HC, at a lower extend than PMS. Progressive patients had higher LF than relapsing remitting ones ($F(1,34) = 5.64$, $p = .02$) (Table 2).

Two-way MANOVAs testing for group differences revealed that vector of means was different across groups for each parameter: MT [Wilks' Lambda = 0.50, $F(6,128) = 8.92$, $p < .001$, $R^2 = 0.50$], R1 [Wilks' Lambda = 0.67, $F(6,128) = 4.77$, $p < .001$, $R^2 = 0.33$], R2* [Wilks' Lambda = 0.64, $F(6,128) = 5.39$, $p < .0001$, $R^2 = 0.36$]. More specifically, MT in NACGM and NAWM was lower in patients than in HC, suggesting a demyelination in these normal appearing tissue classes. Patient groups did not significantly differ from each other, although MT in these two tissue classes tended to be lower in PMS group. In NADGM, MT was lower in PMS patients than in HC (Fig. 3). R2* and R1 from NACGM and NAWM were lower in patients than in HC suggesting reduction of myelin and/or iron content. Patient groups did not significantly differ from each other (Fig. 3). We did not observe any increase of R2* in NADGM between HC and patients. The group by scan interaction was significant for R2* [Wilks' Lambda = 0.80, $F(6,128) = 3.06$, $p < .007$, $R^2 = 0.20$], due to a simple, or ordinal, interaction in NACGM and NAWM for R2*.

There was no significant correlation between qMRI parameters and LF in the RRMS group. In PMS patients, R1 was negatively correlated to LF in NACGM ($r = -0.7$, $p < .001$) and in NAWM ($r = -0.72$, $p < .001$). Regarding BPF, we observed positive correlation with MT in NACGM ($r = 0.65$, $p < .001$), NADGM ($r = 0.63$, $p = .002$) and NAWM ($r = 0.62$, $p = .002$). Positive correlations with BPF were also noted for R1 in NADGM ($r = 0.62$, $p = .002$), R2* in NACGM ($r = 0.65$, $p = .001$) and R2* in NAWM ($r = 0.64$, $p = .004$).

Stepwise regression identified that LF and R2* in NADGM are the best predictors of motor score. It also revealed that cognitive score is best predicted by LF and MT parameter within lesions. Finally, R2* in NADGM and R1 in NACGM predict EDSS (Table 3). Simple linear regressions illustrate these relationships (Fig. 4). Slopes did not differ between groups of patients except for motor score with lesion load. This simple linear regression was stronger in RRMS ($R^2 = 0.58$, $p = .001$) than PMS patients ($R^2 = 0.1$, $p = .24$). By contrast, simple regression between EDSS and R2* in NADGM was significant in the PMS group

Table 2
Quantitative MR parameters.

Groups	RRMS	PMS	HC
Scanner 1/Scanner 2	11/4	15/6	11/25
Volumetric Data, %, mean (SD)			
BPF	84.99 (2.02)	83.67 (2.47)[b]	85.39 (1.75)
GMF	51.06 (2.11)	48.49 (3.16)[b]	52.76 (1.99)
Lesion F	1.21 (0.98)[a]	2.26 (1.50)	N/A
Median MPM values, mean (SD)			
MT (p.u)			
NACGM	0.71 (0.09)[c]	0.68 (0.09)[b]	0.82 (0.09)
NADGM	0.91 (0.12)	0.83 (0.10)[b]	0.98 (1.13)
NAWM	1.49 (0.18)[c]	1.45 (0.16)[b]	1.68 (0.14)
Lesion	0.96 (0.26)	0.89 (0.24)	N/A
R2* (Hz)			
NACGM	15.20 (1.19)[c]	15.35 (1.17)[b]	16.62 (1.02)
NADGM	20.74 (2.63)	22.46 (2.94)	22.04 (3.10)
NAWM	20.08 (1.34)[c]	20.24 (1.27)[b]	21.60 (1.03)
Lesion	15.03 (2.23)	14.51 (2.30)	N/A
R1 (Hz)			
NACGM	0.62 (0.02)[c]	0.61 (0.03)[b]	0.64 (0.02)
NADGM	0.75 (0.05)	0.75 (0.05)	0.77 (0.06)
NAWM	0.99 (0.05)[c]	0.99 (0.05)[b]	1.04 (0.03)
Lesion	0.78 (0.12)	0.75 (0.10)	N/A

Abbreviations: BPF = brain parenchymal fraction, GMF = grey matter fraction, Lesion F = lesion fraction, NACGM = normal appearing cortical grey matter, NADGM = normal appearing deep grey matter, NAWM = normal appearing white matter, N/A = not applicable.

[a] Difference between RRMS and PMS statistically significant (alpha value of 0.05).

[b] Difference between PMS and HC statistically significant (alpha value of 0.05).

[c] Difference between RRMS and HC statistically significant (alpha value of 0.05).

(R^2 = 0.23, p = .03) but not in the RRMS group (R^2 = 0.003, p = .9).

4. Discussion

In this prospective cross-sectional study, quantitative MRI (qMRI) based on a multiparameter mapping (MPM) protocol derives fully quantitative and reproducible (Weiskopf et al. 2013) high-resolution maps of multiple parameters (MT, R2*, R1) from data acquired in a single scanning session of clinically acceptable duration (Tabelow et al. 2019). Dedicated toolboxes for qMRI in the presence of lesions (*hMRI* and *USwithLesion*) were successfully applied to the data. Expectedly, median values of all parameters in HC are similar to those reported in other studies evaluating the MPM protocol (Table 2) (Callaghan et al. 2014; Weiskopf et al. 2013). By contrast to volumetric analyses, mainly interested in lesion topography and regional brain atrophy, the multivariate qMRI approach characterizes microstructural features in 4 different tissue classes (NACGM, NADGM, NAWM and lesions), providing informative proxies about diffuse pathogenic changes such as demyelination or iron deposition. On average, MS patients are characterized by a decrease in MT, R2* and R1 within NACGM and NAWM, whereas in NADGM, MT decrease contrasts with normal R2* and R1 values.

Magnetization transfer is usually assessed by MTR, a semi-quantitative estimation of the steady-state MRI signal attenuation by an off-resonance MT pulse (Helms et al. 2010). Here we quantified MT saturation, which differs from MTR by explicitly removing the bias introduced by the spatially varying T1 relaxation time and B1-transmit field (Helms et al. 2010). The reduction of NAWM and NACGM MT in MS concords with similar observations based on MTR, which is reduced in normal appearing brain tissues of MS patients, particularly in PMS patients (Filippi and Agosta 2007; Jurcoane et al. 2016). MT was also selectively decreased in PMS within NADGM. This result tallies with the demyelination reported post-mortem within NADGM (Haider et al.

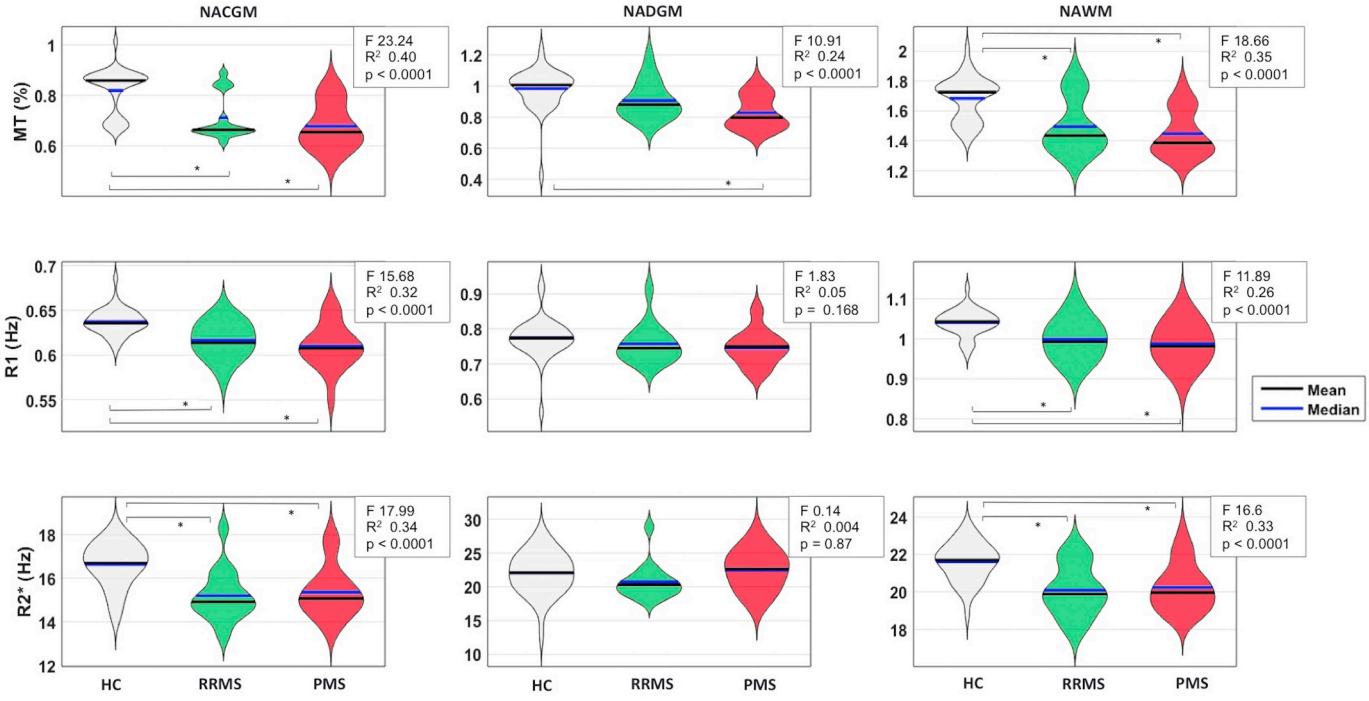

Fig. 3. Violin plots and results of post-hoc analysis.
Plots and post-hoc results for each parameter (MT, R1, R2*) in each tissue class (NACGM, NADGM NAWM), across the 3 groups of subjects (HC, RRMS, PMS). Statistical significance (*) set at $p < .05$.

Table 3
Stepwise regression results (significant level for entry into the model 0.05).

	Model	F (4,31) = 7.18 ($p < .001$)					
	Step	Predictor	ΔR^2	R^2	Adj R^2	ΔF	p Value
Motor score	1	Age and scanner[a]	0.30	0.30	0.25	6.97	.003
	2	Lesion F	0.11	0.4	0.35	5.82	.02
	3	R2* NADGM	0.08	0.48	0.42	4.51	.04
	Model	F (4,30) = 11.99 ($p < .001$)					
	Step	Predictor	ΔR^2	R^2	Adj R^2	ΔF	p Value
Cognitive score	1	Age and scanner[a]	0.22	0.22	0.17	4.42	.02
	2	Lesion F	0.34	0.56	0.52	24.12	< .001
	3	MT Lesion	0.06	0.61	0.56	4.32	.04
	Model	F (4,31) = 8.33 ($p < .001$)					
	Step	Predictor	ΔR^2	R^2	Adj R^2	ΔF	p Value
EDSS	1	Age and scanner[a]	0.35	0.35	0.31	8.70	< .001
	2	R2* NADGM	0.09	0.44	0.39	5.27	.03
	3	R1 NACGM	0.08	0.52	0.46	5.15	.03

Significant level for entry into the model = .05.
Abbreviations: NACGM = normal appearing cortical grey matter, NADGM = normal appearing deep grey matter, Lesion F = lesion fraction, EDSS = expanded disability status scale.
[a] Forced into the model.

2014; Kutzelnigg et al. 2005; Schmierer et al., 2004, 2007) which contributes to clinical deficits over and above cerebral cortical and WM lesion burden (DeLuca et al. 2015; Haider et al. 2014).

Effective transverse relaxation rate R2* is primarily affected by iron, local myelin content, fiber orientation, and water content (Bagnato et al. 2018; Cohen-Adad 2014). R2* is decreased in MS NACGM and NAWM, suggesting a reduction in iron or myelin content, in keeping with histopathological (Hametner et al. 2013) and MR evidence (Bagnato et al. 2018; Hernández-torres et al. 2015; Neema et al. 2007; Paling et al. 2012; Reitz et al. 2016). In contrast to previous reports (Elkady et al. 2017; Khalil et al., 2009, 2011; Ropele et al. 2014), we did not observe any significant increase in R2* parameter in NADGM in MS patients. Although we do not have any clear explanation for this negative result, it might arise from a residual effect age on R2*, RRMS patients being younger than HC. However, age difference was not statistically significant between PMS patients and HC. In any case, the lack of difference in R2* cannot be explained by atrophy in deep grey matter (Hernández-torres et al. 2018), as our method is not confounded by tissue class volume.

Longitudinal relaxation rate R1 is closely related to tissue myelination, particularly in NACGM and NAWM (Neema et al. 2007; Sereno et al. 2013; Stüber et al. 2014), as well as water content and iron concentration (Ogg and Steen 1998). In this study, we observed a reduction of R1 in NACGM and NAWM in both patient groups, indicating a diffuse demyelination in these normal appearing tissues, as previously reported (Gracien et al. 2016; Jurcoane et al. 2016; Neema et al. 2007; Vrenken et al. 2006). No significant change in NADGM R1 was observed either because there was no significant demyelination or iron deposition or because demyelination (which reduces R1) was compensated by increased iron (which increases R1).

4.1. Relation to clinical measures and lesion fraction

This study probes both focal (FLAIR positive lesions) and diffuse microstructural aspects (qMRI parameters) altered by MS, although the latter are to some extent confounded by GM lesions to which MPM protocol is insensitive at 3 Tesla.

Both focal and diffuse processes relate to disability in MS patients. Stepwise regressions indicate that qMRI features are independent predictors of clinical status, supporting the role of diffuse microstructural alterations in clinical impairment: EDSS is significantly related to R1 in NACGM and R2* in NADGM; the latter also predicts motor score. The

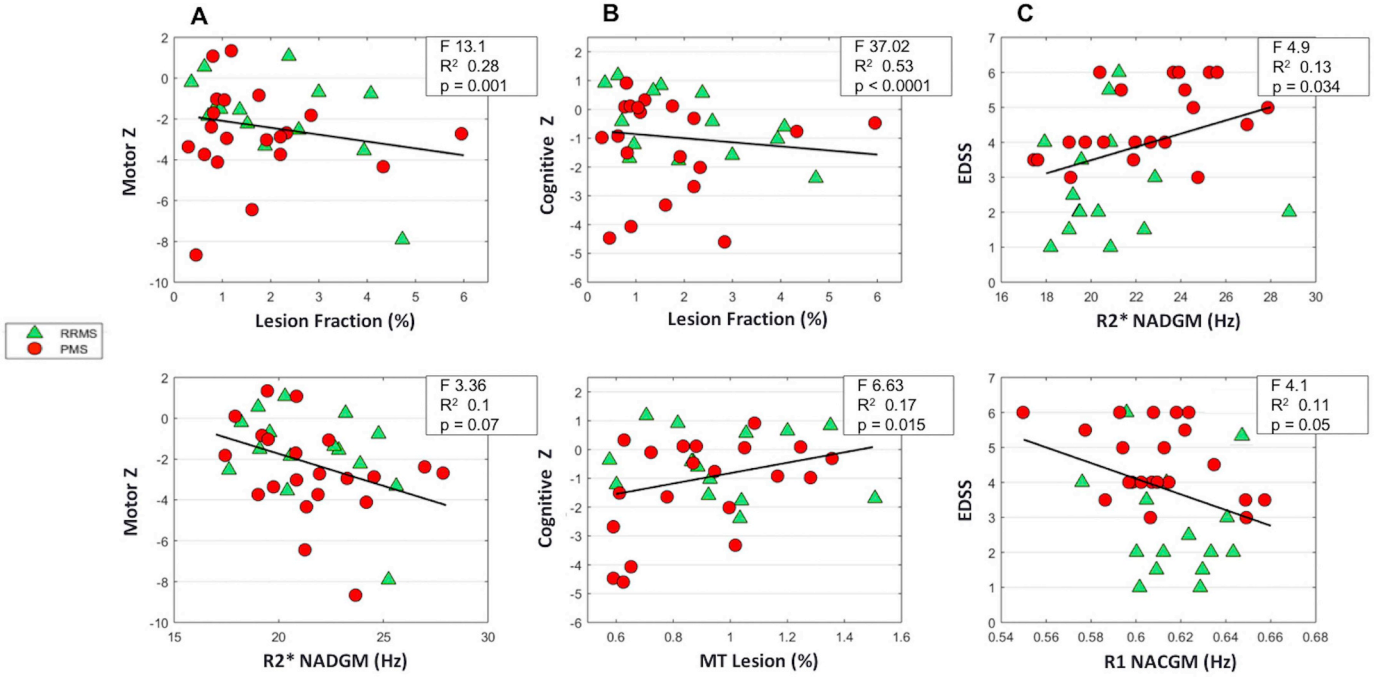

Fig. 4. Interconnections between quantitative MR parameters and clinical scores across the entire group of MS patients.
(A) Simple linear regression between motor score and lesion fraction or R2* within NADGM; (B) simple linear regression between cognitive score and lesion fraction or MT within lesions; (C) simple linear regression between EDSS and R2* within NADGM or R1 within NACGM. Statistical significance set at $p < .05$.

information added by qMRI parameters over and above lesion load might here appear trivial in patients with fairly long disease durations. However, the time course of microstructural alterations during disease evolution might provide predictive information early on in the evolution of the disease, independently from lesion load. This has to be assessed in future studies. Likewise, cognitive score was intriguingly related to MT within lesions. This finding suggests that cognition not only depends on the spatial extension of the lesions (Giorgio and De Stefano, 2010) but also on the pathogenic mechanisms going on within them, which putatively deteriorate axonal transmission to a variable extent.

By the same token, although cohort sizes did not allow us to consider RRMS and PMS separately in our stepwise regression model, simple regressions showed that the motor score depended significantly more on LF in the RRMS group and EDSS more strongly on NADGM R2* in PMS patients. Based on these findings, it is tantalizing to postulate that focal demyelination primarily impacts RRMS clinical status whereas diffuse inflammation and the resulting neurodegeneration mainly cause disability progression in PMS. Specifically, data from literature highlight the role of NADGM involvement in disability accumulation in MS, that tends to be even more evident in PMS (Eshaghi et al. 2018; Haider et al. 2014; Mesaros et al. 2011; Ropele et al. 2014). By contrast, no association between LF and qMRI parameters was observed in RRMS, suggesting the partial independence of diffuse and focal processes. Conversely, R1 in NACGM and NAWM was negatively correlated to LF in PMS, implying that as lesion load increases, the focal and diffuse changes become indistinguishable and jointly impact the clinical status.

Finally, most qMRI parameters in NABT correlated with brain volume loss and might turn out to be useful markers of neurodegeneration. As for the lesion load, future studies will assess whether alterations of qMRI parameters precede atrophy. Importantly, quantitative reproducible microstructural parameters might prove more reliable than the estimation of atrophy (Amiri et al. 2018; Azevedo and Pelletier 2016).

4.2. Limitations of this study

This study is not without limitations. Beyond the small sample size, significant differences in age were observed with older PMS than RRMS patients. However, a linear effect of age was included in our statistical models. Moreover, the disease duration was comparable in the 2 groups, minimizing any effect of this factor.

Although the use of 2 scanners might appear as a drawback, we considered it as the opportunity to test the stability of qMRI parameters across devices, all the more because there were minor differences between the two acquisition protocols due to optimization of several parameters on the second scanner. We found a group by scanner interaction only for R2* in NAGGM and NAWM. These were ordinal, or simple, interactions: scanner data are not parallel across group but never cross. In other words, the group effect can still reliably be discussed.

The automatic unified segmentation approach, with and without WM lesions, ensures the systematic and reproducible processing of both patients and controls data. Consequently, it may be affected by noise and artifacts in the data, which would lead to the spurious classification of a few voxels. Nevertheless, since the median over all the voxels having a strong posterior probability ($> .9$) of being in a tissue class (NACGM, NADGM or NAWM) is used to build the summary measurements, for each subject and qMRI parameter, these should be fairly insensitive to outlier values. At worst this would introduce some between participant variability reducing the sensitivity of the analysis.

5. Conclusion

This cross-sectional study demonstrates that simultaneous quantitative estimation of multiple MR parameters can reliably assess NABT microstructure in MS. Results suggest that diffuse pathology, as assessed by this study, might play a significant role in determining irreversible disability and brain volume loss in MS. However, future large-scale studies should evaluate the reproducibility and predictive values of these results and explicitly discriminate the respective effects of diffuse cortical pathology from focal cortical lesions. Because each qMRI parameter is differentially sensitive to myelin and iron, this multivariate qMRI approach might prove superior to any one single-parameter relaxometry by characterizing each patient, tissue class or voxel in a multidimensional quantitative space.

Declaration of conflicting interests

The author(s) declared no potential conflicts of interest with respect to the research, authorship, and/or publication of this article.

Funding

E.L and C·P are supported by the Fonds de la Recherche Scientifique (F.R.S.-FNRS Belgium).

Research ethics and patient consent

Informed consent for patient information and images to be published was provided by the patient.

Acknowledegements

The authors are particularly thankful for the patients and healthy controls who eagerly took part in this study.

Appendix A. Supplementary data

Supplementary data to this article can be found online at https://doi.org/10.1016/j.nicl.2019.101879.

References

Amiri, H., Sitter, A. De, Bendfeldt, K., Battaglini, M., Wheeler-kingshott, C.A.M.G., Calabrese, M., Geurts, J.J.G., Rocca, M.A., Sastre-garriga, J., Enzinger, C., Stefano, N. De, Filippi, M., Rovira, Á., Barkhof, F., Vrenken, H., Group, M.S, 2018. Urgent challenges in quantification and interpretation of brain grey matter atrophy in individual MS patients using MRI. NeuroImage Clin. 19, 466–475. https://doi.org/10.1016/j.nicl.2018.04.023.

Ashburner, J., Friston, K.J., 2005. Unified segmentation. Neuroimage 26, 839–851.

Azevedo, C.J., Pelletier, D., 2016. Whole-brain atrophy: ready for implementation into clinical decision-making in multiple sclerosis? Curr. Opin. Neurol. 29 (3), 237–242. https://doi.org/10.1097/WCO.0000000000000322.

Bagnato, F., Hametner, S., Boyd, E., Endmayr, V., Shi, Y., Ikonomidou, V., Chen, G., Pawate, S., Lassmann, H., Smith, S., Brian Welch, E., 2018. Untangling the R2* contrast in multiple sclerosis: a combined MRI-histology study at 7.0 Tesla. PLoS One 13, 1–19. https://doi.org/10.1371/journal.pone.0193839.

Balteau, E., Leutritz, T., Weiskopf, N., Reimer, E., Lutti, A., Callaghan, M.F., et al., 2018. Evaluating T2* bias impact and correction strategies in quantitative proton density mapping. In: Poster Presented at Joint Annual Meeting ISMRM-ESMRMB, Paris, France.

Barkhof, F., 2002. The clinico-radiological paradox in multiple sclerosis revisited. Curr. Opin. Neurol. 15, 239–245. https://doi.org/10.1097/00019052-200206000-00003.

Callaghan, M.F., Freund, P., Draganski, B., Anderson, E., Cappelletti, M., Chowdhury, R., Diedrichsen, J., Fitzgerald, T.H.B., Smittenaar, P., Helms, G., Lutti, A., Weiskopf, N., 2014. Widespread age-related differences in the human brain microstructure revealed by quantitative magnetic resonance imaging. Neurobiol. Aging 35, 1862–1872. https://doi.org/10.1016/j.neurobiolaging.2014.02.008.

Cohen-Adad, J., 2014. What can we learn from T2* maps of the cortex? Neuroimage 93, 189–200. https://doi.org/10.1016/j.neuroimage.2013.01.023.

DeLuca, G.C., Yates, R.L., Beale, H., Morrow, S.A., 2015. Cognitive impairment in multiple sclerosis: clinical, radiologic and pathologic insights. Brain Pathol. 25, 79–98. https://doi.org/10.1111/bpa.12220.

Draganski, B., Ashburner, J., Hutton, C., Kherif, F., Frackowiak, R.S.J., Helms, G., Weiskopf, N., 2011. Regional specificity of MRI contrast parameter changes in normal ageing revealed by voxel-based quantification (VBQ). Neuroimage 55, 1423–1434. https://doi.org/10.1016/j.neuroimage.2011.01.052.

Elkady, A.M., Cobzas, D., Sun, H., Blevins, G., Wilman, A.H., 2017. Progressive iron accumulation across multiple sclerosis phenotypes revealed by sparse classification of

deep gray matter. J. Magn. Reson. Imaging 46, 1464–1473. https://doi.org/10.1002/jmri.25682.
Enzinger, C., Barkhof, F., Ciccarelli, O., Filippi, M., Kappos, L., Rocca, M.A., Ropele, S., Rovira, À., Schneider, T., Stefano, N. De, Vrenken, H., 2015. Cerebral changes in multiple sclerosis. Nat. Publ. Gr. 11, 676–686. https://doi.org/10.1038/nrneurol.2015.194.
Eshaghi, A., Brownlee, W.J., Altmann, D.R., Tur, C., Cardoso, M.J., De Angelis, F., Van De Pavert, S.H., Cawley, N., De Stefano, N., Stromillo, M.L., Battaglini, M., Ruggieri, S., Gasperini, C., Filippi, M., Rocca, M.A., Rovira, A., Killestein, J., Pirpamer, L., Enzinger, C., Ourselin, S., Wheeler-kingshott, C.A.M.G., Chard, D., Thompson, A.J., Alexander, D.C., 2018. Deep Gray Matter Volume Loss Drives Disability Worsening in Multiple Sclerosis. Ann Neurol. 83, 210–222. https://doi.org/10.1002/ana.25145.
Filippi, M., Agosta, F., 2007. Magnetization transfer MRI in multiple sclerosis. J. Neuroimaging 17 (Suppl. 1), 22S–26S. https://doi.org/10.1111/j.1552-6569.2007.00132.x.
Filippi, M., Rocca, M.A., Barkhof, F., Brück, W., Chen, J.T., Comi, G., Deluca, G., Stefano, N. De, Erickson, B.J., Evangelou, N., Fazekas, F., Geurts, J.J.G., Lucchinetti, C., Miller, D.H., Pelletier, D., Popescu, B.F.G., 2012. Association between pathological and MRI findings in multiple sclerosis. Lancet Neurol. 11, 349–360. https://doi.org/10.1016/S1474-4422(12)70003-0.
Filippi, M., Rocca, M.A., Horsfield, M.A., Hametner, S., Geurts, J.J.G., Comi, G., Lassmann, H., 2013. Imaging cortical damage and dysfunction in multiple sclerosis. JAMA Neurol. 70, 556–564. https://doi.org/10.1001/jamaneurol.2013.1954.
Giorgio, A., De Stefano, N., 2010. Cognition in multiple sclerosis: relevance of lesions, brain atrophy and proton MR spectroscopy. Neurol. Sci. 31, 245–248. https://doi.org/10.1007/s10072-010-0370-x.
Gracien, R.M., Reitz, S.C., Hof, S.M., Fleischer, V., Zimmermann, H., Droby, A., Steinmetz, H., Zipp, F., Deichmann, R., Klein, J.C., 2016. Changes and variability of proton density and T1 relaxation times in early multiple sclerosis: MRI markers of neuronal damage in the cerebral cortex. Eur. Radiol. 26, 2578–2586. https://doi.org/10.1007/s00330-015-4072-x.
Haider, L., Simeonidou, C., Steinberger, G., Hametner, S., Grigoriadis, N., Deretzi, G., Kovacs, G.G., Kutzelnigg, A., Lassmann, H., Frischer, J.M., 2014. Multiple sclerosis deep grey matter: the relation between demyelination, neurodegeneration, inflammation and iron. J. Neurol. Neurosurg. Psychiatry 85, 1386–1395. https://doi.org/10.1136/jnnp-2014-307712.
Hametner, S., Wimmer, I., Haider, L., Pfeifenbring, S., Brück, W., Lassmann, H., 2013. Iron and neurodegeneration in the multiple sclerosis brain. Ann. Neurol. 74, 848–861. https://doi.org/10.1002/ana.23974.
Helms, G., Dathe, H., Dechent, P., 2010. Modeling the influence of TR and excitation flip angle on the magnetization transfer ratio (MTR) in human brain obtained from3D spoiled gradient echoMRI. Magn. Reson. Med. 64, 77–185.
Hernández-torres, E., Wiggermann, V., Hametner, S., 2015. Orientation dependent MR signal decay differentiates between people with MS, their asymptomatic siblings and unrelated healthy controls. PLoS One 21, 1–14. https://doi.org/10.1371/journal.pone.0140956.
Hernández-torres, E., Wiggermann, V., Machan, L., Sadovnick, A.D., Li, D.K.B., Traboulsee, A., Hametner, S., Rauscher, A., 2018. Increased mean R2* in the deep gray matter of multiple sclerosis patients: have we been measuring atrophy? J. Magn. Reson. Imaging. https://doi.org/10.1002/jmri.26561. (Epub ahead of print).
Hulst, H.E., Geurts, J.J.G., 2011. Gray matter imaging in multiple sclerosis: what have we learned? BMC Neurol. 11. https://doi.org/10.1186/1471-2377-11-153.
Jurcoane, A., Wagner, M., Reitz, S.C., Mayer, C., Volz, S., Hof, S., Fleischer, V., Droby, A., Steinmetz, H., Groppa, S., Hattingen, E., Deichmann, R., Klein, J.C., 2016. Multimodal Quantitative MRI Assessment of Cortical Damage in Relapsing-Remitting Multiple Sclerosis. J. Magn. Reson. Imaging 44, 1600–1607. https://doi.org/10.1002/jmri.25297.
Khalil, M., Enzinger, C., Langkammer, C., Tscherner, M., Wallner-Blazek, M., Jehna, M., Ropele, S., Fuchs, S., Fazekas, F., 2009. Quantitative assessment of brain iron by R(2)* relaxometry in patients with clinically isolated syndrome and relapsing-remitting multiple sclerosis. Mult. Scler. 15, 1048–1054. https://doi.org/10.1177/1352458509106609.
Khalil, M., Langkammer, C., Ropele, S., Petrovic, K., Wallner-Blazek, M., Loitfelder, M., Jehna, M., Bachmaier, G., Schmidt, R., Enzinger, C., Fuchs, S., Fazekas, F., 2011. Determinants of brain iron in multiple sclerosis: a quantitative 3T MRI study. Neurology 77, 1691–1697. https://doi.org/10.1212/WNL.0b013e318236ef0e.
Kutzelnigg, A., Lucchinetti, C.F., Stadelmann, C., Bruck, W., Rauschka, H., Bergmann, M., Schmidbauer, M., Parisi, J.E., Lassmann, H., 2005. Cortical demyelination and diffuse white matter injury in multiple sclerosis. Brain 128, 2705–2712. https://doi.org/10.1093/brain/awh641.
Lorio, S., Fresard, S., Adaszewski, S., Kherif, F., Chowdhury, R., Frackowiak, R.S., Ashburner, J., Helms, G., Weiskopf, N., Lutti, A., Draganski, B., 2016. New tissue priors for improved automated classification of subcortical brain structures on MRI. Neuroimage 130, 157–166. https://doi.org/10.1016/j.neuroimage.2016.01.062.
Lutti, A., Hutton, C., Finsterbusch, J., Helms, G., Weiskopf, N., 2010. Optimization and validation of methods for mapping of the radiofrequency transmit field at 3T. Magn. Reson. Med. 64, 229–238. https://doi.org/10.1002/mrm.22421.
Lutti, A., Stadler, J., Josephs, O., Windischberger, C., Speck, O., Bernarding, J., Hutton, C., Weiskopf, N., 2012. Robust and fast whole brain mapping of the RF transmit field B1 at 7T. PLoS One 7, 1–7. https://doi.org/10.1371/journal.pone.0032379.
Mesaros, S., Rocca, M. a, Pagani, E., Sormani, M.P., Petrolini, M., Comi, G., Filippi, M., 2011. Thalamic damage predicts the evolution of primary-progressive multiple sclerosis at 5 years. AJNR Am. J. Neuroradiol. 32, 1016–1020. https://doi.org/10.3174/ajnr.A2430.
Miller, D.H., Leary, S.M., 2007. Primary-progressive multiple sclerosis. Lancet Neurol. 6, 903–912. https://doi.org/10.1016/S1474-4422(07)70243-0.
Moon, N., Bullitt, E., Leemput, K. Van, Gerig, G., 2002. Automatic Brain and Tumor Segmentation. MICCAI, Tokyo, pp. 1–5.
Neema, M., Stankiewicz, J., Arora, A., Dandamudi, V.S.R., Batt, C.E., Guss, Z.D., Al-Sabbagh, A., Bakshi, R., 2007. T1- and T2-based MRI measures of diffuse gray matter and white matter damage in patients with multiple sclerosis. J. Neuroimaging 17, 16–21. https://doi.org/10.1111/j.1552-6569.2007.00131.x.
Ogg, R.J., Steen, R.G., 1998. Age-related changes in brain T1 are correlated with iron concentration. Magn. Reson. Med. 40, 749–753. https://doi.org/10.1002/mrm.1910400516.
Paling, D., Tozer, D., Wheeler-Kingshott, C., Kapoor, R., Miller, D.H., Golay, X., 2012. Reduced R2' in multiple sclerosis normal appearing white matter and lesions may reflect decreased myelin and iron content. J. Neurol. Neurosurg. Psychiatry 83, 785–792. https://doi.org/10.1136/jnnp-2012-302541.
Phillips, C., Lommers, E., Pernet, C., 2017. Unifying lesion masking and tissue probability maps for improved segmentation and normalization. In: Poster, 23rd Annu. Meet. Organ. Hum. Brain Mapping, Vancouver, Canada.
Polman, C.H., Reingold, S.C., Banwell, B., Clanet, M., Cohen, J.A., Filippi, M., Fujihara, K., Havrdova, E., Hutchinson, M., Kappos, L., Lublin, F.D., Montalban, X., O'Connor, P., Sandberg-Wollheim, M., Thompson, A.J., Waubant, E., Weinshenker, B., Wolinsky, J.S., 2011. Diagnostic criteria for multiple sclerosis: 2010 revisions to the McDonald criteria. Ann. Neurol. 69, 292–302. https://doi.org/10.1002/ana.22366.
Preibisch, C., Deichmann, R., 2009. Influence of RF spoiling on the stability and accuracy of T1 mapping based on spoiled FLASH with varying flip angles. Magn. Reson. Med. 61, 25–135.
Reich, D.S., Lucchinetti, C.F., Calabresi, P.A., 2018. Multiple sclerosis. N. Engl. J. Med. 378, 169–180. https://doi.org/10.1056/NEJMra1401483.
Reitz, S.C., Hof, S., Fleischer, V., Brodski, A., Gröger, A., Gracien, R., Droby, A., Steinmetz, H., 2017. Multi-parametric quantitative MRI of normal appearing white matter in multiple sclerosis, and the effect of disease activity on T2. Brain Imaging Behav. 11, 744–753. https://doi.org/10.1007/s11682-016-9550-5.
Ropele, S., Kilsdonk, I.D., Wattjes, M.P., Langkammer, C., De Graaf, W.L., Frederiksen, J.L., Larsson, H.B., Yiannakas, M., Wheeler-Kingshott, C.A.M., Enzinger, C., Khalil, M., Rocca, M.A., Sprenger, T., Amann, M., Kappos, L., Filippi, M., Rovira, A., Ciccarelli, O., Barkhof, F., Fazekas, F., 2014. Determinants of iron accumulation in deep grey matter of multiple sclerosis patients. Mult. Scler. J. 20, 1692–1698. https://doi.org/10.1177/1352458514531085.
Schmidt, P., Gaser, C., Arsic, M., Buck, D., Förschler, A., Berthele, A., Hoshi, M., Ilg, R., Schmid, V.J., Zimmer, C., Hemmer, B., Mühlau, M., 2012. An automated tool for detection of FLAIR-hyperintense white-matter lesions in multiple sclerosis. Neuroimage 59, 3774–3783. https://doi.org/10.1016/j.neuroimage.2011.11.032.
Schmierer, K., Scaravilli, F., Altmann, D.R., Barker, G.J., Miller, D.H., 2004. Magnetization transfer ratio and myelin in postmortem multiple sclerosis brain. Ann. Neurol. 56, 407–415. https://doi.org/10.1002/ana.20202.
Schmierer, K., Tozer, D.J., Scaravilli, F., Altmann, D.R., Barker, G.J., Tofts, P.S., Miller, D.H., Daniel, R., Barker, G.J., Tofts, P.S., Miller, D.H., 2007. Quantitative magnetization transfer imaging in postmortem multiple sclerosis brain. J. Magn. Reson. Imaging 26, 41–51. https://doi.org/10.1002/jmri.20984.
Sereno, M.I., Lutti, A., Weiskopf, N., Dick, F., 2013. Mapping the human cortical surface by combining quantitative T1 with retinotopy. Cereb. Cortex 23, 2261–2268. https://doi.org/10.1093/cercor/bhs213.
Stüber, C., Morawski, M., Schäfer, A., Labadie, C., Wähnert, M., Leuze, C., Streicher, M., Barapatre, N., Reimann, K., Geyer, S., Spemann, D., Turner, R., 2014. Myelin and iron concentration in the human brain: a quantitative study of MRI contrast. Neuroimage 93, 95–106. https://doi.org/10.1016/j.neuroimage.2014.02.026.
Tabelow, K., Balteau, E., Ashburner, J., Callaghan, M.F., Draganski, B., Helms, G., Kherif, F., Leutritz, T., Lutti, A., Phillips, C., Reimer, E., Ruthotto, L., Seif, M., Weiskopf, N., Ziegler, G., Mohammadi, S., 2019. hMRI – a toolbox for quantitative MRI in neuroscience and clinical research. Neuroimage 194, 191–210.
Vrenken, H., Geurts, J.J., Knol, D.L., van Dijk, L.N., Dattola, V., Jasperse, B., van Schijndel, R.A., Polman, C.H., Castelijns, J.A., Barkhof, F., Pouwels, P.J., 2006. Whole-brain T1 mapping in multiple sclerosis: global changes of normal-appearing gray and white matter. Radiology 240, 811–820. https://doi.org/10.1148/radiol.2403050569.
Weiskopf, N., Suckling, J., Williams, G., Correia, M., Inkster, B., Tait, R., Ooi, C., Bullmore, T.E., Lutti, A., 2013. Quantitative multi-parameter mapping of R1, PD*, MT, and R2* at 3T: a multi-center validation. Front. Neurosci. 7, 1–11. https://doi.org/10.3389/fnins.2013.00095.
Weiskopf, N., Callaghan, M.F., Josephs, O., Lutti, A., Mohammadi, S., 2014. Estimating the apparent transverse relaxation time (R2*) from images with different contrasts (ESTATICS) reduces motion artifacts. Front. Neurosci. 8, 1–10. https://doi.org/10.3389/fnins.2014.00278.
Zivadinov, R., Leist, T.P., 2005. Clinical-magnetic resonance imaging correlations in multiple sclerosis. J. Neuroimaging 15, 10S–21S. https://doi.org/10.1177/1051228405283291.